DE GRUYTER

Chemical Papers 69 (8) 1033–1043 (2015)
DOI: 10.1515/chempap-2015-0110

ORIGINAL PAPER

Integrated investigations for the characterisation of Roman lead-glazed pottery from Pompeii and Herculaneum (Italy)

[a]Lorena Carla Giannossa, [b]Daniela Fico*, [b]Antonio Pennetta, [a]Annarosa Mangone, [c]Rocco Laviano, [b]Giuseppe Egidio De Benedetto

[a]*Department of Chemistry,* [c]*Department of Earth and Geoenvironmental Sciences, University of Bari Aldo Moro, via Orabona 4, 70126 Bari, Italy*

[b]*Laboratory of Analytical and Isotopic Mass Spectrometry, Department of Cultural Heritage, University of Salento, campus Ecotekne, s.p. Lecce-Monteroni, 73100, Lecce, Italy*

Received 24 October 2014; Revised 12 January 2015; Accepted 3 February 2015

A multi-analytical approach was used to investigate Roman lead-glazed ceramic artefacts from archaeological excavations at Pompeii and Herculaneum (Italy) aiming at defining the production technology of both glaze and ceramic body, by way of integrated investigations. The chemical, structural, and micro-morphological characterisations were performed using a combination of laser ablation-inductively coupled plasma-mass spectrometry (LA-ICP-MS), optical microscopy (OM), scanning electron microscopy (SEM), and micro-Raman spectroscopy. Fragments of artefacts (skyphoi, oil lamps, bowls, askoi, amphorae, krateres) of great historical and archaeological interest were sampled. LA-ICP-MS was used to determine the elemental composition by virtue of its effective lateral resolution, its ability to detect most elements and also to analyse comparably small samples. All the archaeological objects were coated with a lead-based glaze produced using a lead oxide-plus-quartz mixture, with sodium/potassium feldspars added as a flux and two different metals used: copper and iron. Two types of ceramic pastes have been identified, but chemometric techniques support the hypothesis of a Campanian provenance for the raw materials. Degradation phenomena such as the partial devitrification of the glaze, i.e. the slow structural reorganisation towards stable crystalline phases, and the leaching by mineral dissolution in the soil, were determined.

Keywords: laser ablation, pottery, principal component analysis, production technology, multi-analytical approach

Introduction

The practice of coating pottery is attested from ancient times and it was developed for aesthetic and functional purposes, for instance to effect both brightness and waterproofing. Among the different classes of artefacts excavated in Pompeii and Herculaneum, an interesting nucleus of lead-glazed pottery, representing the largest set of lead-glazed pottery analysed to date, was selected for their historical and aesthetic relevance. The stable production of lead-glazed pottery and its distribution arrived from the East in the first century BC (Desbat, 1995; Génin et al., 1996; Hochuli-Gysel, 2002; Di Gioia, 2006). Records of the European production of lead-glazed pottery are quite scarce and are concentrated in Italy and France (near Lyon) up to the Augustan period (Desbat, 1995, 1986). Only in the second half of the first century AD did glazed pottery spread to Britain, Spain, and the Danube basin (Walton & Tite, 2010; Arthur, 1979; Picon & Desbat, 1986; Martin, 1992).

As regards northern Italy, it is assumed that, in

*Corresponding author, e-mail: daniela.fico@unisalento.it

addition to the import of pottery from the workshops of Tarsus, there was a widespread local production (Maccabruni, 1987, 1994). Ateliers producing glazed pottery have also been hypothesised (Greene, 2007; De Benedetto et al., 2004; Soricelli, 1988) for central and southern Italy (Lazio and Campania) and, as no production centres have as yet been identified in these regions, both the production technology and the provenance of this class of pottery are of great interest.

Two primary glazing technologies have been proposed for Roman pottery: either the application of a lead compound or a mixture of a lead compound and quartz onto the ceramic body (Walton & Tite, 2010). Slight variants of these two procedures were also used, such as the addition of clays to the glaze or the application of the glazing material onto uncooked or fired ceramic bodies. A comparison of the chemical and mineralogical composition of glaze and body (Walton & Tite, 2010; Hurst & Freestone, 1996) is required to distinguish between these methods.

The elemental composition of the ceramic bodies, the lead isotopic patterns of the glaze, together with stylistic and petrographic data are generally used to establish provenance. The chemical composition of the body was used to hypothesise as to the provenance of artefacts of unknown origin (Pérez-Arantegui et al., 1996; Picon & Vichy, 1974; Hatcher et al., 1994), while lead isotopic patterns were often used to reinforce the data interpretation (Walton & Tite, 2010).

The objects of the present research were twenty-six samples of glazed pottery from the Pompeii and Herculaneum areas, representing the largest set of lead-glazed pottery analysed to date. In order to investigate the provenance, the technical manufacturing aspects (information on the raw materials and their processing), and the deterioration phenomena (the effect of ageing prior to excavation), the microchemical and micro-structural nature of the samples was investigated using a multi-disciplinary approach and a combination of techniques, suitably adapted to the specificity of materials of archaeological interest, e.g. non- or micro-destructive characterisation. In particular, different traditional techniques, including polarising optical microscopy (OM), scanning electron microscopy coupled with an energy-dispersive X-ray spectrometer (SEM-EDS), and micro-Raman spectroscopy (Raman), were used in combination with laser ablation-inductively coupled plasma-mass spectrometry (LA-ICP-MS).

In the last decade, LA-ICP-MS has emerged as affording spatial control, important in these structurally heterogeneous samples, analysis speed, thanks to the absence of the need for chemical dissolution of samples, and micro-sampling, also providing knowledge of elemental composition when the quantity of sam-

Table 1. List of Roman lead-glazed pottery samples where the glaze and ceramic body were analysed

Sample	Inventory	Stored	Description	Glaze colour
1	14820[b]	Pompeii excavation deposit	Handle	Dark green
2	13168[b]	Pompeii excavation deposit	Oil lamp	Green
3	19078[c]	Pompeii deposit	Oil lamp	Green
4	10732[b]	Pompeii deposit	Oil lamp	Dark green
5	3262[b]	Pompeii deposit	Oil lamp	Dark green
6	4910[b]	Pompeii deposit	Oil lamp	Dark green
7	7229[b]	Pompeii deposit	Oil lamp	Dark green
8	6587A[b]	Pompeii deposit	Fragment	Brown-ochre
9	17777[b]	Pompeii deposit	Filter	Brown-ochre
10[a]	11502[b]	Pompeii deposit	Askos	Brown-ochre
11	19818[c]	Pompeii deposit	Bowl	Brown-ochre
12	19814[b]	Pompeii deposit	Bowl	Green out/brown-ochre in
13	19300[c]	MANN[e]	Oil lamp	Green
14	no inventory[c]	MANN[e] deposit	Askos	Green
15[a]	116669[b]	MANN[e]	Amphora	Dark green
16	22544[c]	MANN[e]	Oil lamp	Green
17	76937-1659[d]	Herculaneum deposit	Amphora	Brown-ochre
18	79322[c]	Herculaneum deposit	Fragment	Green
19	no inventory[d]	Pompeii deposit	Fragment	Green
20	1578[b]	Pompeii deposit	Bowl	Green out/brown-ochre in
21	12431[b]	Pompeii deposit	Calyx-Krater	Green out/brown-ochre in
22	11978[b]	Pompeii deposit	Askos	Dark green
23	11771[b]	Pompeii deposit	Skyphos	Green out/brown-ochre in
24	19817[c]	Pompeii deposit	Bowl	Green
25	43623[b]	Pompeii deposit	Skyphohs	Green
26	76-165[b]	MANN[e]	Oil lamp	Green

a) Only glaze analysed; *b*) recovered in Pompeii; *c*) unknown; *d*) recovered in Herculaneum; *e*) National Archaeological Museum of Naples (MANN).

Fig. 1. Image of some samples analysed. Scale bar = 3 cm.

ples is insufficient for a traditional ICP-MS analysis; it is now extensively used by archaeometrists in chemical studies (James et al., 2005; Resano et al., 2005; Cochrane & Neff, 2006; Mangone et al., 2009, 2011a; van Elteren et al., 2009; Šelih & van Elteren, 2011; Stoner & Glascock, 2012) and was used in the present study to selectively sample glaze, body and deterioration of the different samples. In respect of the OM, SEM, and Raman analyses, specifically, OM was used to obtain information on the structure and texture of the ceramic bodies (e.g. presence of mineral phases, lithic fragments, etc.) and the glazes (e.g. presence of phases of neoformation, bubbles, craquelure, etc.). SEM-EDS analysis was employed in a morphological–structural investigation to evaluate the conservation state, to identify the mineralogical accessory phases in the ceramic bodies and the structure and thickness of the coatings. Micro-Raman analysis was used to investigate the crystalline phases, to classify the glass matrix and to obtain information on the firing temperatures of glazes, calculating the polymerisation index (Colomban et al., 2004, 2006).

Experimental

The samples examined consisted of finds, codified in Table 1, recovered during archaeological excavations carried out in the last century at the sites of Pompeii and Herculaneum (Italy) and stored in Pompeii -Casa di Bacco-, in the archaeological deposit of the Superintendence of Herculaneum and in the National Archaeological Museum of Naples (MANN).

The objects (bowls, lamps, skyphoi, askoi, etc.) were extensively studied from the archaeological perspective (Di Gioia, 2006). All finds were characterised by a green (dark or light) and/or brown-ochre coating, and by a red ceramic body (Fig. 1).

Small fragments of already damaged objects were used for the analyses, thus minimising the perceptible effect. This circumstance restricted the range of analytical techniques that could be employed, due to the quantity of the sample useful for the investigations. Therefore, for all the objects, it was not always possible to sample both the ceramic body and the glaze.

The fragments were examined using different complementary techniques: OM, SEM-EDS, micro-Raman spectroscopy, and LA-ICP-MS.

Examination of the mineralogical texture was performed by means of an optical microscope (Axioscop 40 – Carl Zeiss, Oberkochen, Germany) on polished thin sections, whereas SEM (LEO EVO-50XVP, Zeiss, Cambridge, UK) investigations were carried out on both untreated samples and on polished thin sections, after graphite sputter-coating. Microanalyses were conducted using an Oxford-Link EDS instrument (Oxford Instruments, High Wycombe, UK) equipped with a PENTAFET (Si) detector and with a 0.4-mm-thick Super atmosphere thin window (SATW).

The micro-Raman spectra were recorded using a Renishaw Invia instrument (Renishaw, York, UK)

Table 2. Operating conditions and data acquisition parameters used for LA-ICP-MS analysis

ICP-MS gas flows	Coolant (plasma)	Ar: 13 L min^{-1}
	Auxiliary	Ar: 0.7 L min^{-1}
	Sample transport	He: ca 0.5 L min^{-1} (in ablation cell), Ar (make up gas flow): ca 0.7 L min^{-1}
Laser	Wavelength	213 nm (Nd:YAG)
	Pulse width (FWHM)	3 ns
	Energy distribution	Homogenised, flat beam, aperture imaged
	Energy density (fluence) on sample surface	10 J cm^{-2}
	Focus	Fixed at surface
	Repetition rate	5 Hz
	Crater diameter	ca 32 μm (10 μm for interaction layer and interparticle glass)
	Line scan speed	20 μm s^{-1}
Analysis protocol	Scanning mode	Peak jumping, 1 point per peak, 10 ms dwell time
	Acquisition mode	Time-resolved analysis
	Analysis duration	120 s (ca 60 s background, 30 s signal, 30 s washout)
	Isotopes monitored	^{7}Li, ^{9}Be, ^{23}Na, ^{24}Mg, ^{27}Al, ^{29}Si, ^{39}K, ^{44}Ca, ^{47}Ti, ^{51}V, ^{52}Cr, ^{55}Mn, ^{57}Fe, ^{59}Co, ^{60}Ni, ^{65}Cu, ^{66}Zn, ^{75}As, ^{85}Rb, ^{88}Sr, ^{90}Zr, ^{93}Nb, ^{107}Ag, ^{111}Cd, ^{115}In, ^{118}Sn, ^{121}Sb, ^{138}Ba, ^{139}La, ^{140}Ce, ^{141}Pr, ^{146}Nd, ^{147}Sm, ^{153}Eu, ^{157}Gd, ^{159}Tb, ^{163}Dy, ^{165}Ho, ^{166}Er

equipped with both diode (785 nm) and He–Cd (325 nm and 442 nm) lasers. Two objectives 20× and 50× (Leica DM LM microscope, Leica Microsystems, Wetzlar, Germany) were used to focus the laser beam on the samples and to receive the back-scattered Raman signal. The exposure time and the accumulations were selected on a case-by-case basis to obtain sufficiently informative spectra; five scans, 20 s each, were generally used. The wavelength scale was calibrated using a Si(111) standard (520.5 cm^{-1}). The crystalline phases were identified by comparison with the library of standard spectra acquired on the same apparatus.

The laser ablation system employed in this study was a New Wave Research UP213AI 213 nm (ESI-New Wave Research Co., Cambridge, UK). This solid sampling device was coupled to a Thermo Electron X series II (Thermo Electron Corporation, Waltham, USA), a quadrupole-based ICP-MS with an enhanced sensitivity Xs-interface. The ICP-MS was optimised for dry plasma conditions prior to each analytical session in continuous linear ablation mode on NIST SRM 612 by maximising the signals for selected masses (Mg+, Sr+, and Th+) and reducing oxide formation by minimising the ThO+/Th+ ratio. Helium was flushed into the ablation cell to reduce the deposition of ablated aerosols and to improve signal intensities and mixed with argon prior to entering the plasma torch through a Y-shaped HDPE connector: this configuration made it possible to maintain stable and optimal excitation conditions and enhanced transport efficiency of the ablated material. Analyses were performed on the polished cross-sections under the operating conditions given in Table 2.

To overcome the analyte- and matrix-dependent elemental response variations in LA-ICP-MS, different calibration approaches using a single (Šelih & van Elteren, 2011) or multiple (van Elteren et al., 2009; Halicz & Günther, 2004; Liu et al., 2008) standards were proposed and validated. Given that clay and glaze composition had to be determined in a single experiment, the ablation yield correction factor (AYCF) approach (Liu et al., 2008) was used and the factors were calculated using NIST 610, BCR RM126A, and Corning D glasses and pelleted NIST Silica brick 199 and Brick clay 679 standards. The LOD were calculated using the 3s criterion for the actual laser beam of ø 32 μm from the signal of NIST616 standard and are reported in Tables 3 and 4. Accuracy, expressed as the relative difference between the recorded and the reference values of NIST 612 and Corning C standards, was greater than 10 % for all the elements.

Due to the sample heterogeneity (clay compounds, including minerals and fillers), the LA-ICP-MS analyses were carried out performing ablation on multiple patterns: in particular, up to nine lines, 32 μm wide and not less than 1 mm long, were selected for the ceramic body on each sample at the microscope, in an attempt to exclude volcanic minerals and rock fragments, and ablated. As the glazes were more homogeneous, only three lines were ablated. Tables 3, 4, and S1 show the mean composition and standard deviation for ceramic bodies and glazes, respectively.

Principal component analysis (PCA) and clustering analysis was carried out on standardised data using the software package Minitab®.

Table 3. Major constituents of glaze bodies and relevant standard deviation (σ) calculated considering all scans performed expressed as mass % (LA-ICP-MS results)

Sample	Na_2O		MgO		Al_2O_3		SiO_2		K_2O		CaO		TiO_2		Fe_2O_3		CuO		PbO_2	
	mass %		mass %		mass %		mass %		mass %		mass %		mass %		mass %		mass %		mass %	
	Mean	σ	Mean	σ	Mean	σ	Mean	σ	Mean	σ	Mean	σ	Mean	σ	Mean	σ	Mean	σ	Mean	σ
1 (9 lines)	0.3	0.1	0.46	0.07	4.5	0.5	36.1	3.1	0.10	0.03	4.6	0.8	0.20	0.03	0.16	0.03	2.38	0.31	51	6
2 (9 lines)	0.8	0.2	0.88	0.11	6.6	0.8	35.7	3.1	0.92	0.19	5.3	0.9	0.15	0.02	1.15	0.15	2.06	0.27	46	5
3 (9 lines)	0.3	0.1	0.27	0.04	3.9	0.5	32.6	2.8	0.40	0.11	2.3	0.5	0.09	0.01	0.85	0.14	3.71	0.48	55	4
4 (9 lines)	0.3	0.1	0.26	0.04	5.4	0.6	31.0	2.7	1.03	0.21	2.5	0.5	0.16	0.02	0.86	0.14	2.27	0.29	56	4
5 (8 lines)	0.3	0.1	0.30	0.05	2.4	0.4	38.6	2.9	0.15	0.04	2.2	0.5	0.07	0.01	0.80	0.13	5.04	0.56	50	6
6 (9 lines)	0.2	0.1	0.12	0.02	1.6	0.2	35.4	3.0	0.38	0.10	2.0	0.4	0.08	0.01	0.79	0.13	1.63	0.26	58	5
7 (9 lines)	0.3	0.1	0.29	0.04	1.6	0.2	27.2	2.4	0.05	0.01	3.7	0.6	0.07	0.01	0.40	0.07	3.28	0.43	63	5
8 (9 lines)	0.4	0.1	0.38	0.06	5.7	0.7	26.0	2.3	0.04	0.01	2.0	0.4	0.11	0.02	0.90	0.15	0.01	0.01	64	5
9 (9 lines)	0.5	0.1	0.50	0.08	9.0	1.0	32.5	2.8	0.67	0.14	1.7	0.4	0.34	0.04	2.22	0.29	0.02	0.01	52	6
10 (9 lines)	0.9	0.2	0.16	0.02	9.2	1.1	35.2	3.0	0.08	0.02	5.7	1.0	0.05	0.01	1.94	0.26	0.05	0.01	46	5
11 (9 lines)	0.2	0.1	0.49	0.07	9.4	1.0	36.7	3.2	0.69	0.14	3.5	0.6	0.32	0.05	0.98	0.13	0.01	0.01	48	5
12r (9 lines)	0.5	0.1	0.43	0.07	3.8	0.5	28.8	2.5	0.89	0.19	2.5	0.5	0.23	0.03	1.66	0.22	0.08	0.01	61	5
12g (9 lines)	0.3	0.1	0.30	0.05	2.4	0.4	38.6	2.9	0.67	0.14	2.2	0.5	0.07	0.01	0.80	0.13	5.04	0.56	49	6
13 (9 lines)	0.7	0.2	0.46	0.07	3.3	0.5	37.4	3.2	0.14	0.04	3.0	0.6	0.23	0.04	0.28	0.05	4.18	0.54	50	6
14 (9 lines)	0.4	0.1	0.17	0.03	0.6	0.1	20.3	2.2	0.63	0.13	1.4	0.3	0.04	0.01	0.34	0.06	2.67	0.35	73	6
15 (7 lines)	0.4	0.1	0.13	0.02	0.6	0.1	35.1	3.0	0.14	0.04	1.9	0.4	0.03	0.01	0.30	0.05	4.36	0.56	57	4
16 (9 lines)	0.4	0.1	0.20	0.03	1.6	0.2	30.0	2.6	0.18	0.05	2.7	0.6	0.04	0.01	0.51	0.09	5.02	0.65	59	5
17 (9 lines)	0.7	0.2	0.40	0.06	6.5	0.8	26.7	2.3	0.90	0.19	1.6	0.3	0.24	0.04	1.62	0.22	0.02	0.01	61	5
18 (9 lines)	0.7	0.2	1.78	0.19	5.0	0.6	36.5	3.1	1.68	0.30	5.8	1.0	0.27	0.04	0.88	0.15	2.11	0.27	45	5
19 (9 lines)	2.0	0.4	0.27	0.04	3.9	0.5	36.6	3.1	0.72	0.15	7.3	1.1	0.10	0.02	0.99	0.13	1.99	0.26	46	5
20g (9 lines)	0.8	0.2	0.37	0.06	2.4	0.3	35.0	3.0	1.26	0.26	3.3	0.7	0.18	0.03	0.99	0.13	2.54	0.33	53	6
20r (8 lines)	2.7	0.5	0.51	0.08	6.4	0.8	32.1	2.8	1.08	0.23	7.3	1.2	0.95	0.10	1.80	0.24	0.04	0.01	47	5
21 (9 lines)	0.4	0.1	0.32	0.05	1.4	0.2	31.7	2.7	0.17	0.04	2.4	0.5	0.11	0.02	0.09	0.02	2.25	0.29	61	5
22 (9 lines)	0.6	0.2	0.35	0.05	7.7	0.9	38.6	3.3	0.14	0.04	6.2	1.1	0.06	0.01	0.19	0.03	2.17	0.28	44	5
23g (7 lines)	0.8	0.2	0.35	0.05	2.4	0.4	38.0	3.3	0.71	0.15	4.2	0.7	0.14	0.02	1.04	0.14	1.99	0.26	50	6
23r (8 lines)	1.5	0.3	0.93	0.11	5.2	0.6	38.3	3.3	1.34	0.28	4.9	0.8	0.29	0.04	2.87	0.33	0.10	0.02	44	5
24 (9 lines)	0.5	0.1	0.63	0.08	3.9	0.5	32.9	2.8	0.15	0.04	4.9	0.8	0.33	0.04	0.26	0.04	1.06	0.17	55	4
25 (9 lines)	0.2	0.1	0.03	0.01	2.2	0.3	17.8	1.9	0.13	0.03	3.4	0.6	0.01	0.01	0.02	0.01	1.19	0.19	75	4

Results and discussion

Ceramic body

Macroscopically, all the ceramic bodies show a red colour and a porous paste, with dark clasts visible in some samples (Di Gioia, 2006); however, the apparent macroscopic homogeneity does not accord with a microscopic homogeneity of pastes since different mineral-petrographic characteristics can be recognised. The red-glazed ceramic potsherds are characterised by a non-calcareous paste with remarkable amounts of iron oxides and mineral inclusions, almost all of quartz and feldspar.

The other potsherds, by contrast, exhibit a calcareous paste with volcanic minerals, lithic fragments and raw materials indicative of volcanic origin: sanidine, biotite, and forsterite plus Ti-andradite (melanite garnet), pyroxenes (frequently green diopside), volcanoclastic and pumice fragments (Fig. 2). These volcanic fragments and minerals (i.e. melanite garnet and diopside) exhibit characteristics ascribable to the magmatic Campanian area (Pompeii, Campi Flegrei, or Monte Somma). Within this group, two subgroups were differentiated on the strength of dimension and quantity of volcanic minerals and lithic fragments, rare and small (< 100 μm) or common and large (> 100 μm) (Fig. 2).

A firing temperature of approximately 950 ℃, maintained for at least sufficient time to complete the reaction between the clayey minerals and calcite, may be deduced during the firing process for the last group (the calcareous one), thanks to the identification, in different samples, of gehlenite; for the first group (the red glazed one), the well-sintered pastes support the hypothesis of the use of a firing temperature higher than 900 ℃ (Heimann & Maggetti, 1981).

The elemental composition, obtained from LA-ICP-MS analysis (Table S1, see Supplementary Data) was processed by multivariate statistical techniques, Principal components analysis (PCA) and Clustering analysis, to recognise groups of samples characterised by way of their elemental composition. To carry out a more effective chemometric analysis, lead and copper elemental data were excluded from the dataset: their presence in the glazes could be discriminating, taking into consideration not their chemical nature or the ratio of the mixture of the materials utilised but the

Table 4. Minor constituents of glaze bodies and relevant standard deviation (σ) calculated considering all scans performed expressed as $\mu g\ g^{-1}$ (LA-ICP-MS results)

Sample	V_2O_5		Cr_2O_3		MnO		CoO		NiO		ZnO		As_2O_3		SrO		SnO_2		Sb_2O_5		BaO	
	$\mu g\ g^{-1}$		$\mu g\ g^{-1}$		$\mu g\ g^{-1}$		$\mu g\ g^{-1}$		$\mu g\ g^{-1}$		$\mu g\ g^{-1}$		$\mu g\ g^{-1}$		$\mu g\ g^{-1}$		$\mu g\ g^{-1}$		$\mu g\ g^{-1}$		$\mu g\ g^{-1}$	
	Mean	σ	Mean	σ	Mean	σ	Mean	σ	Mean	σ	Mean	σ	Mean	σ	Mean	σ	Mean	σ	Mean	σ	Mean	σ
1 (9 lines)	262	68	26	7	360	80	1	1	10	2	338	54	68	24	128	27	20	5	224	37	158	29
2 (9 lines)	213	55	216	49	394	87	5	2	190	43	134	27	9	3	138	23	2	1	25	4	73	13
3 (9 lines)	73	19	17	5	206	46	2	1	77	17	53	11	23	8	61	13	7	2	80	13	42	8
4 (9 lines)	88	23	10	5	2208	387	3	1	73	16	66	13	27	10	131	28	183	46	139	23	74	13
5 (8 lines)	55	14	24	7	241	53	2	1	135	31	79	16	35	13	57	12	5	1	92	15	28	5
6 (9 lines)	173	45	16	5	1662	294	1	1	136	31	17	5	172	49	237	40	13	3	53	9	18	3
7 (9 lines)	88	23	15	5	185	41	3	1	33	8	38	8	36	13	67	14	7	2	63	10	36	6
8 (9 lines)	166	43	27	8	180	40	3	1	31	7	65	13	9	3	56	12	2	1	36	6	133	24
9 (9 lines)	191	49	90	25	227	50	5	2	92	21	218	43	35	12	111	24	10	3	140	23	193	35
10 (9 lines)	106	27	230	52	288	64	9	4	72	16	45	9	222	63	100	21	626	159	911	120	29	5
11 (9 lines)	500	103	28	8	144	32	2	1	12	3	80	16	44	16	264	44	2	1	90	15	162	29
12r (9 lines)	118	30	240	53	240	53	12	4	105	24	209	41	38	14	134	28	58	15	30	5	118	21
12g (9 lines)	55	14	24	7	241	53	2	1	135	31	79	16	35	13	57	12	5	1	92	15	28	5
13 (9 lines)	80	21	50	14	310	68	2	1	10	2	166	48	110	31	80	17	10	3	650	86	90	16
14 (9 lines)	44	11	14	5	2299	403	1	1	60	14	72	14	15	5	49	10	27	7	92	15	34	6
15 (7 lines)	41	11	28	8	121	27	2	1	120	27	85	17	270	77	56	12	2626	460	1310	150	24	4
16 (9 lines)	48	12	19	5	357	79	2	1	100	23	142	28	56	20	57	12	163	41	285	47	18	3
17 (9 lines)	880	157	148	33	302	67	11	5	71	16	98	19	51	18	167	28	146	37	17	3	364	53
18 (9 lines)	420	87	147	33	2915	445	17	5	85	19	200	40	119	34	299	50	1970	397	518	69	177	32
19 (9 lines)	258	66	55	16	449	99	8	4	287	52	539	86	8	3	186	32	401	102	247	41	133	24
20g (9 lines)	102	26	74	21	336	74	17	5	139	32	300	48	100	29	168	29	100	25	335	55	967	121
20r (8 lines)	277	71	352	68	526	116	11	5	38	9	842	115	6	2	177	30	237	60	159	26	169	31
21 (9 lines)	48	12	58	16	114	25	32	9	22	5	86	17	146	42	110	23	1192	242	308	51	58	10
22 (9 lines)	155	40	157	35	639	141	16	5	59	13	124	25	89	32	98	21	71	18	828	110	20	4
23g (7 lines)	107	28	93	26	159	35	8	4	90	20	91	18	67	24	193	33	2020	407	360	60	197	36
23r (8 lines)	372	77	300	67	477	105	23	7	21	5	240	48	288	81	311	46	231	59	244	40	410	59
24 (9 lines)	544	112	92	26	318	70	10	5	56	13	86	17	70	25	178	30	264	67	60	10	106	19
25 (9 lines)	78	20	14	5	281	62	2	1	28	6	81	16	36	13	77	16	700	178	52	9	9	2

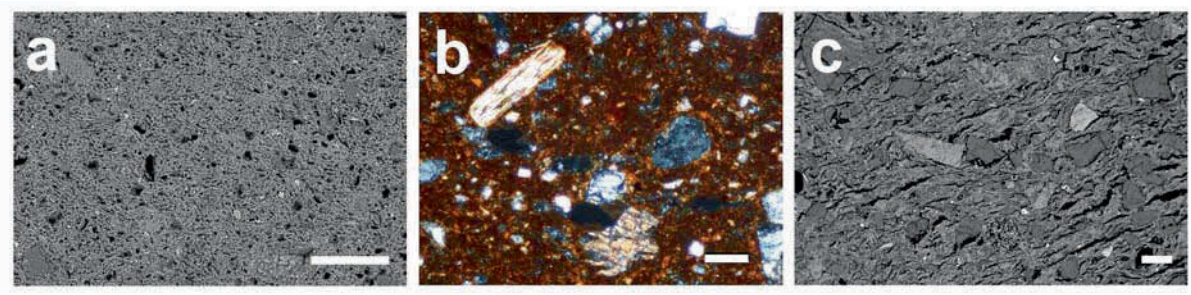

Fig. 2. SEM-BSE photomicrograph of ceramic body of sample 9 (a). OM (b) and SEM-BSE (c) photomicrographs of ceramic body of sample 15. Scale bar = 100 μm.

possible diffusion processes during the firing from the surface to the ceramic body and vice versa (Molera et al., 2001).

Prior to PCA treatment, statistical criteria of selecting features were also applied, e.g. comparison of means and variances of the variables, which led to deletion of the few parameters bearing just noise to the analysis. For example, elements such as Na, Ti, Sr, and Mn were eliminated; in these cases, the mean was quite similar for every predicted class and/or the intra-class variance was high. In this way, a highly distinct class structure was found by PCA. The selected elements were Mg, Al, Si, K, Ca, Cr, Fe, Ni.

The scores and loadings overlay plot onto the first three principal components subspace, which accounts for 76 % of the total variance, is shown in Fig. 3, thereby identifying three clusters (A, B, and C). In detail, the split between the samples of cluster A and the others two clusters is observed along the PC1 (A scores are characterised by negative values of PC1, B and C scores by positive values), the further subdivision of cluster B and C is observed along PC2 (C

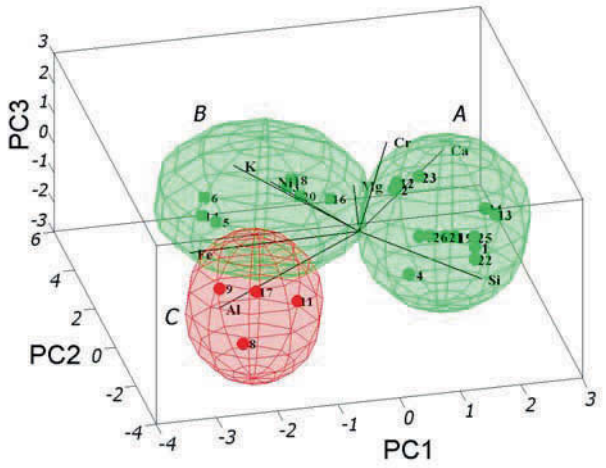

Fig. 3. Scores and loadings diagram for first three principal components related to clayey matrices of fragments. Accounted variance is 76 % of total.

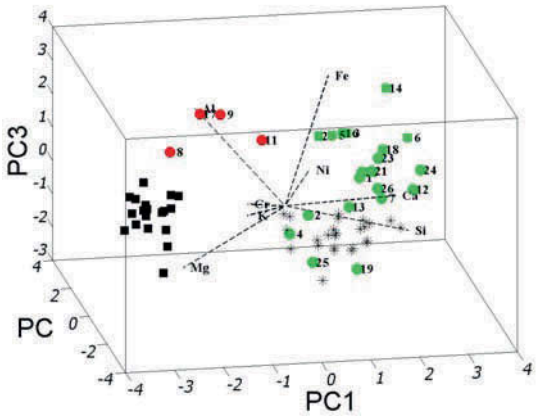

Fig. 4. Scores and loadings diagram for first three principal components related to clayey matrices of thin-walled pottery from Pompeii and Herculaneum fragments (unnumbered) and glazed pottery. Accounted variance is 83 % of total.

scores are characterised by negative values of PC2 and B scores by positive values).The separation of clusters along PC1 is principally due to the loadings relative to the Al, K, and Fe parameters, and along PC2 to Si, Mg and Ca values. The iso-probability ellipsoids, corresponding to a 95 % confidence level, are also shown in Fig. 3. The surface defined by each ellipsoid can be assumed to determine the boundary of each cluster.

In accordance with the results of SEM investigations, the division of objects belonging to cluster C from those belonging to clusters A and B appears to be due to the use of two different raw materials (absence of pyroxenes in samples of cluster C and their presence in both cluster A and B). The distinction between A and B could be linked to differences in the production technology (same mineralogical assembly for both clusters but different dimensions of clasts).

The remarkable similarity in the mineral-petrographic composition of the pastes in clusters B and C with the pastes of thin-walled pottery excavated in the same two archaeological areas, coeval and locally produced (Giannossa et al., 2012, 2014; Mangone et al., 2011b), justifies the extension of the multivariate analysis to the ceramic body matrices data of thin-walled pottery. Fig. 4 shows that objects belonging to clusters B and C merge in one of the two clusters highlighted for thin-walled ware, lending weight to their production in the Vesuvian area.

Glaze

Examination of the cross-sections revealed that the glazes, well vitrified, with a thickness ranging between 120 μm and 200 μm and compact structure, show the distinctive presence of Pb.

Irregular surfaces were observed with frequent signs of corrosion and fractures and bubbles, different in size and number. The areas of the corrosion layers reflected some differences: the internal layers were richer in Pb and exhibited a higher Pb/Si ratio

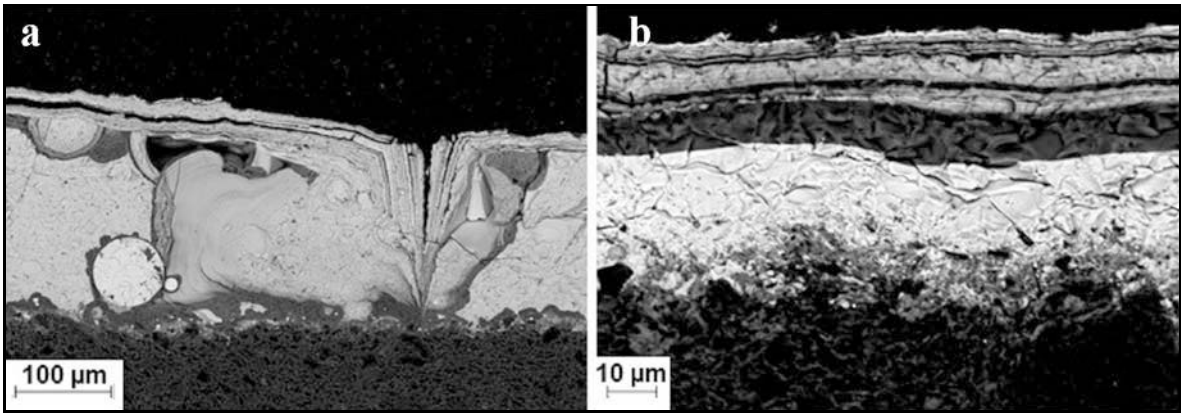

Fig. 5. SEM-BSE photomicrographs of samples 6 (a) and 7 (b) showing irregular surfaces, signs of corrosion, fractures, bubbles, and lead-leaching process.

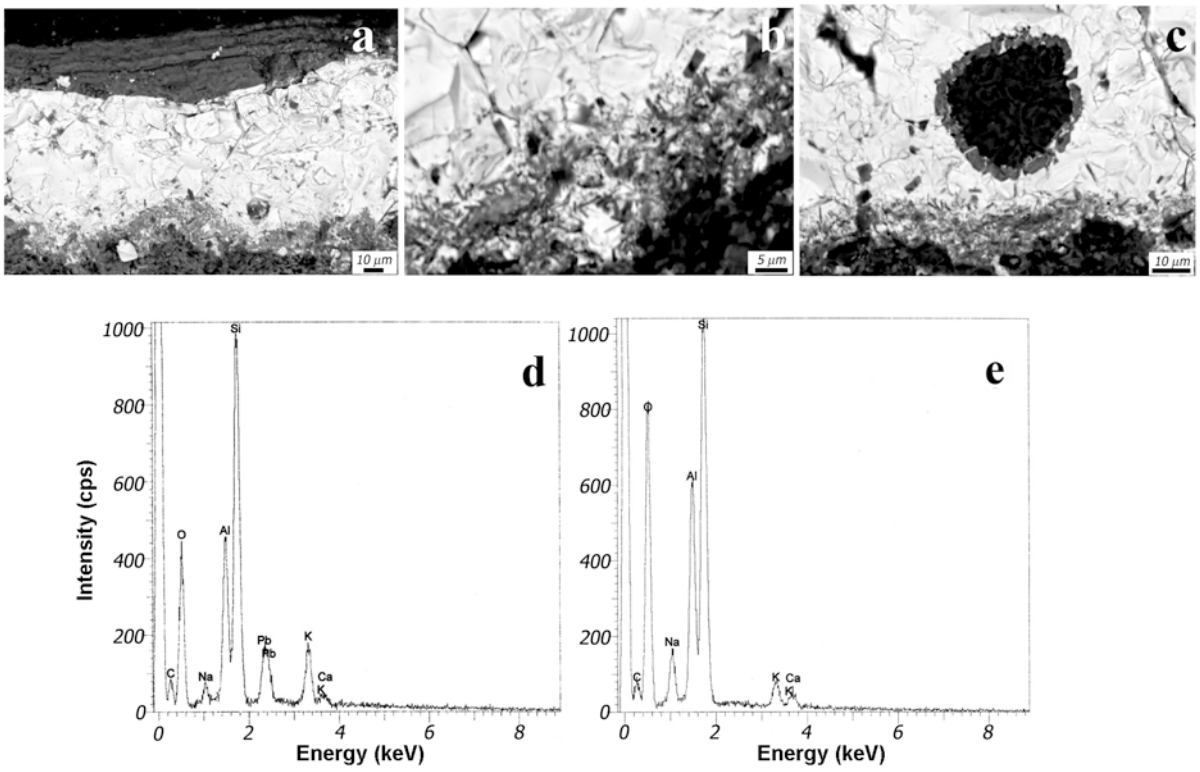

Fig. 6. SEM-BSE photomicrographs of interface glaze-ceramic body (a) and of newly-formed crystals (b) of sample 16. SEM-BSE photomicrograph of hole within glaze (c), ED spectra of external (d), and internal parts (e) of black crystals around hole in sample 26.

than those on the exterior. This was due to the lead-leaching process and was manifested in the lack of the original brilliance of these glazes (Fig. 5). The glaze mass only rarely presented non-fused quartz crystals.

Numerous newly-formed crystals of typical and constant composition, Si, Al, Pb, K, Na are present at the interface glaze-ceramic body (Figs. 6a and 6b). Newly-formed crystals of composition Si, Al, Na, K interior and Si, Al, Pb, K, Na exterior (Figs. 6d and 6e) surrounding a hole (Fig. 6c) were observed within the glaze of sample 26. Their presence and variation in the composition afforded clues to the technological process and the flux employed; a suspension of quartz and lead oxide (probably litharge) with the addition of an alkaline feldspar as flux was possibly used to make the glaze. This hypothesis is indirectly confirmed by the high level of manufacture of these glazes, also documented by the well-sintered ceramic body, obtained at high temperatures.

The results of the elemental analysis by LA-ICP-MS are shown in Tables 3 and 4. The analytical data indicate that the glazes are of the high-lead type, similar in composition to those reported for Roman high-lead glazes by other authors (Hochuli-Gysel, 2002; Picon & Desbat, 1986; Pérez-Arantegui et al., 1996; Hatcher et al., 1994). The total content of PbO varies between 42 mass % and 75 mass %, in accordance with the importance of the processes of lead-leaching, as suggested by the Pb/Si ratio. The presence of copper oxide above 1 mass % in the green glazes (Cu_2O between 1 mass % and 5 mass %), and of iron oxide in the red-brown ones (Fe_2O_3 between 1 mass % and 3 mass %), made it possible to unequivocally attribute the colour to copper- and iron-based compounds, respectively; the different quantities confirm the different shades of colour observed (Walton & Tite, 2010; Greene, 2007; Colomban et al., 2001).

A simultaneous view of the influence of various chemical parameters can be obtained by an analysis of the scores and loadings overlay plot onto the first three principal components subspace, which accounts for 74 % of the total variance (Fig. 7).

In this case also, elements such as Co, As, Sr, and Na were eliminated; in these cases, the mean was substantially the same for every predicted class and/or the intra-class variance was high. In this way, a well-distinguished class structure was found by PCA. The elements selected were Mg, Al, Si, K, Ca, Cr, Fe, Ni. Accordingly, the red glazes differed in composition from the green glazes, in addition to Fe and Cu, mainly for Al, K, Mg, and Ca.

Raman analyses were performed to complete the chemical characterisation of glazes and the typical spectrum of lead-based glazes was always obtained: the main peaks were observed at approximately 500 cm^{-1} (Si—O bending) and 1000 cm^{-1} (Si—O

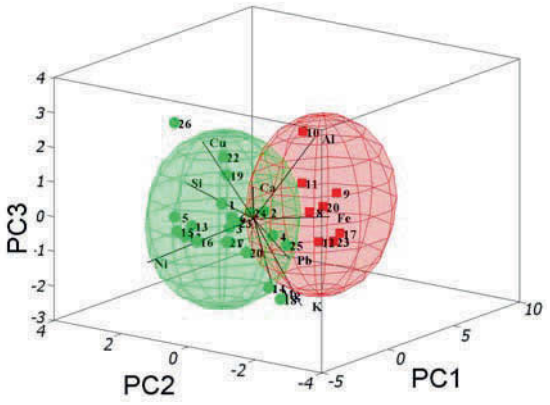

Fig. 7. Scores and loadings diagram for first three principal components related to glazes of Pompeii and Herculaneum fragments. Accounted variance is 74 % of total.

stretching, more intensive in lead glazes) while no specific Raman signature related to chromophores was observed, Fig. 8a (Colomban et al., 2004). As reported in the literature, the band centred at 1000 cm^{-1} of non-crystalline silicates can be deconvoluted as the sum of 4 or 5 bands, one for each Qn component; the relative intensities of these bands can provide a good indication of the degree of polymerisation of a silicate, because of the modification of the partial charge of oxygen atoms involved in the Si—O bonds (Fig. 8a) and of the processing temperature (Colomban et al., 2004, 2006); on the basis of this, a polymerisation index (Ip) (defined as the ratio of the area of the bending band at 500 cm^{-1} and the stretching band at 1000 cm^{-1}) was measured and compared with the reference data. All the glazes showed an Ip between 0.3 and 0.6, values similar to those well documented for lead-rich silicates ($0.3 < Ip < 0.5$) and for lead-based silicates ($0.5 < Ip < 0.8$), hence suggesting a glazing temperature of about 800 °C (Colomban et al., 2004, 2006). These results, which are in good accord with the compositional data obtained by LA-ICP-MS analyses and with the information obtained by SEM-EDS, also confirm that the Raman technique can be a viable alternative to analyses by ICP-MS and EDS for the classification of vitreous bulk, when it is not possible to perform any kind of sampling. However, by using this technique, it is not possible in most cases to identify the elements responsible for colour in the glazes.

In addition, lead carbonate (Raman peak at 1053 cm^{-1}, Fig. 8b) and calcite (Raman peaks at 283 cm^{-1} and 1087 cm^{-1}, Fig. 8b) were identified in some samples (Burgio & Clark, 2001); they could be residues of the raw materials used (lead sulphide

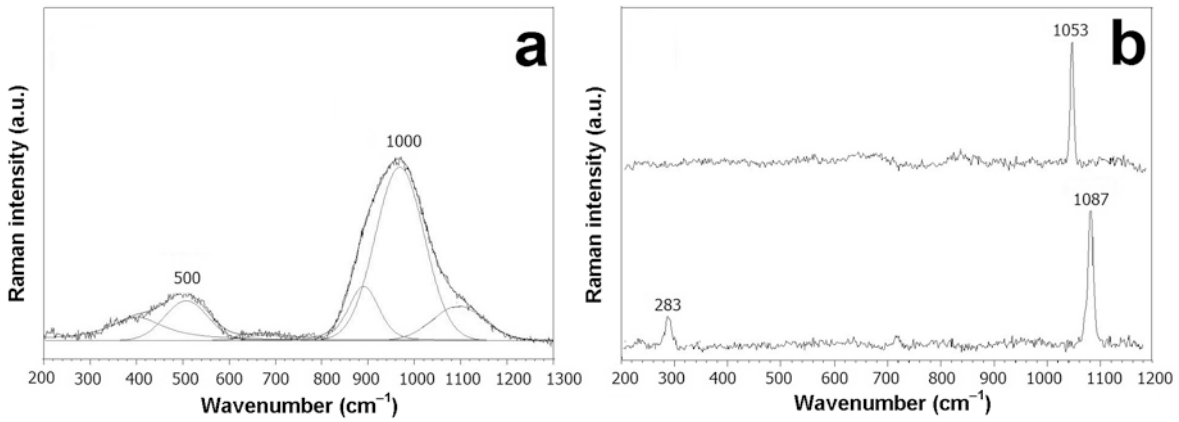

Fig. 8. Raman spectrum of lead glaze and Qn components (a); Raman spectra of lead carbonate and calcite discovered in samples (b).

Table 5. Example of comparison between average values of glaze (after subtraction of % PbO and % CuO or % Fe_2O_3 for green or brown-ochre glaze, respectively, and renormalisation) and ceramic body

Sample		Na_2O	MgO	Al_2O_3	SiO_2	K_2O	CaO	TiO_2	MnO	Fe_2O_3	CuO
		Content/%									
1	Glaze (dark green)	0.68	0.99	9.7	77.5	0.21	9.8	0.43	0.08	0.34	–
	Body	0.77	2.95	16.9	59.9	0.55	16.8	0.77	0.12	0.78	0.02
9	Glaze (brown-ochre)	1.15	1.09	19.8	71.6	1.48	3.8	0.74	0.05	–	0.04
	Body	2.38	1.58	20.2	57.1	3.08	4.9	0.82	0.23	7.13	0.10
19	Glaze (green)	3.76	0.52	7.4	70.2	1.39	14.1	0.19	0.09	1.89	–
	Body	2.90	2.21	13.7	60.9	0.50	15.9	0.23	0.10	1.94	0.02

for example) or the products of glaze weathering (De Benedetto et al., 2004).

As to the methods used to apply the glazes, the two primary glazing methods discussed in the literature (Desbat, 1986, 1995; Génin et al., 1996; Hochuli-Gysel, 2002; Di Gioia, 2006; Walton & Tite, 2010) can be distinguished by subtracting the percentages of lead oxide and copper (or iron) oxide from the glaze composition, and re-normalising the resulting composition to 100 % (Walton & Tite, 2010; De Benedetto et al., 2004); this resulting glaze composition is then compared with the composition of the body (Table 5). When glazing was obtained by the application of lead oxide by itself, the resulting glaze and body compositions should be the same. By contrast, when glazing was produced by the application of a lead oxide-plus-quartz mixture, the silica content of the resulting glaze should be higher than that of the body, and the alumina and other oxide contents should change (Walton & Tite, 2010; De Benedetto et al., 2004). The present results, in good accord with mineral-petrographic data, suggest that the glaze was a mixture of lead oxide and quartz (as for samples 1 and 9 shown in Table 5). In addition, sodium/potassium feldspar could be added in some cases (as for sample 19 in Table 5).

Conclusions

This work details the chemical characterisation of glazed potsherds from the Vesuvian area (Italy): the largest set of lead-glazed pottery analysed from Pompeii and Herculaneum to date, comprising twenty-six finds of different shape and function, was characterised morphologically, mineralogically, and chemically. In addition, clear information emerged on the production technology and raw materials provenance.

Specifically, the ceramic finds were covered with a lead-based glaze produced using a lead oxide-plus-quartz mixture, whereas sodium/potassium feldspars were added as a flux and two different chromophores used: copper for green and iron for yellow-brown glazes.

Although kilns containing glazed ceramic wastes have not yet been discovered, a Campanian provenance for the raw materials is sustained by the chemical and mineral-petrographic data. Besides, the significant similarities in raw materials between the glazed and coeval and locally produced thin-walled pottery originating from Pompeii and Herculaneum (Giannossa et al., 2012, 2014; Mangone et al., 2011b) endorse the hypothesis of a Campanian provenance. As a result, the archaeological thesis that the bilicne oil lamp (sample 26, Fig. 1) was produced in Asia Minor and subsequently imported and glazed in Pompeian workshops, as suggested by archaeologists (Ziviello, 1989) and reported in the museum description at MANN, is contested. The characteristics of the ceramic body and the presence at the interface of the glaze-ceramic body of newly formed crystals of intermediate composition between ceramic body and glaze suggest that the item is an excellent imitation locally produced.

Finally, this study emphasises the growing value of a multidisciplinary approach and the benefits of using LA-ICP-MS in archaeological investigations.

Acknowledgements. This work was performed within the framework of the PRIN 2010-11 (Project no. 2010329WPF_006), and PON 254/Ric. Cod. PONa3_00334, funded by the Italian Ministry for Education, University and Research.

Supplementary data

The supplementary data associated with this article can be found in the online version of this paper (DOI: 10.1515/chempap-2015-0110).

References

Arthur, P. (1979). An Italian flagon from Roman Colchester. *The Antiquaries Journal*, *59*, 392–397. DOI: 10.1017/s00035 81500079786.

Burgio, L., & Clark, R. J. H. (2001). Library of FT-Raman spectra of pigments, minerals, pigment media and vernishes, and supplement to existing library of Raman spectra of pigments with visible excitation. *Spectrochimica Acta Part A: Molecular and Biomolecular Spectroscopy*, *57*, 1491–1521. DOI: 10.1016/s1386-1425(00)00495-9.

Cochrane, E. E., & Neff, H. (2006). Investigating compositional diversity among Fijian ceramics with laser ablation-inductively coupled plasma-mass spectrometry (LA-ICP-MS): implications for interaction studies on geologically similar islands. *Journal of Archaeological Science*, *33*, 378–390. DOI: 10.1016/j.jas.2005.08.003.

Colomban, P., Sagon, G., & Faurel, X. (2001). Differentiation of antique ceramics from the Raman spectra of their coloured glazes and paintings. *Journal of Raman Spectroscopy*, *32*, 351–360. DOI: 10.1002/jrs.704.

Colomban, P., Milande, V., & Le Bihan, L. (2004). On-site Raman analysis of Iznik pottery glazes and pigments. *Journal of Raman Spectroscopy*, *35*, 527–535. DOI: 10.1002/jrs.1163.

Colomban, P., Tournie, A., & Bellot-Gurlet, L. (2006). Raman identification of glassy silicates used in ceramics, glass and jewellery: a tentative differentiation guide. *Journal of Raman Spectroscopy*, *37*, 841–852. DOI: 10.1002/jrs.1515.

De Benedetto, G. E., Acquafredda, P., Masieri, M., Quarta, G., Sabbatini, L., Zambonin, P. G., Tite, M., & Walton, M. (2004). Investigation on Roman lead glaze from Canosa: Results of chemical analyses. *Archaeometry*, *46*, 615–624. DOI: 10.1111/j.1475-4754.2004.00177.x.

Desbat, A. (1986). Céramiques romaines à glaçure plombifère des fouilles de Lyon (Hauts-de-Saint-Just, Rue des Farges, La Solitude). *Figlina*, *7*, 105–124. (in French)

Desbat A. (1995). Les productions précoces de céramiques à glaçure plombifère de la vallée du Rhône. *Rei Cretariae Romanae Fautores Acta*, *34*, 39–47. (in French)

Di Gioia, E. (2006). *La ceramica invetriata in area vesuviana. Studi della Soprintendenza Archeologica di Pompei.* Roma, Italy: L'Erma di Bretschneider. (in Italian)

Génin, D., Desbat, A., Elaigne, S., Laroche, C., & Dangréaux, B. (1996). Les productions de l'atelier de la Muette. *Gallia*, *53*, 41–191. (in French)

Giannossa, L. C., De Benedetto, G. E., Laviano, R., Pallara, M., & Mangone, A. (2012). Archaeometry in the Vesuvian area: Technological teatures of thin-walled ware. In D. Braekmans, J. Honings, & P. Degryse (Eds.), *Proceedings of 39th International Symposium on Archaeometry: 50 years of ISA*, May 28–June 1, 2012 (pp. 157–163). Leuven, Belgium: KU Leuven.

Giannossa, L. C., Acquaviva, M., De Benedetto, G. E., Acquafredda, P., Laviano, R., & Mangone, A. (2014). Methodology of a combined approach: analytical techniques to identify technology and raw materials used in thin-walled pottery from Herculaneum and Pompeii. *Analytical Methods*, *6*, 3490–3499. DOI: 10.1039/c3ay42195c.

Greene, K. (2007). Late Hellenistic and early Roman invention and innovation: The case of lead-glazed pottery. *American Journal of Archaeology*, *111*, 653–671. DOI: 10.3764/aja.111.4.653.

Halicz, L., & Günther, D. (2004). Quantitative analysis of silicates using LA-ICP-MS with liquid calibration. *Journal of Analytical Atomic Spectrometry*, *19*, 1539–1545. DOI: 10.1039/b410132d.

Hatcher, H., Kaczmarczyk, A., Scherer, A., & Symonds, R. P. (1994). Chemical classification and provenance of some Roman glazed ceramics. *American Journal of Archaeology*, *98*, 431–456. DOI: 10.2307/506438.

Heimann, R. B., & Maggetti, M. (1981). Experiments on simulated burial of calcareous Terra Sigillata (mineralogical change). Preliminary results. In M. J. Hughes (Ed.), *Scientific studies in ancient ceramics* (British Museum Occasional Paper 19, pp. 163–177). London, UK: British Museum.

Hochuli-Gysel, A. (2002). La céramique à glaçure plombifère d'Asie Mineure et du bassin méditerranéen oriental (du 1er s. av. J.-C. au 1er s. ap. J.-C.). In F. Blondé, P. Ballet, & J. F. Salles (Eds.), *Céramiques hellénistiques et romaines: Productions et diffusion en Méditerranée orientale (Chypre, Égypte et côte syro-palestinienne)* (Actes du colloque à la Maison de l'Orient méditerranéen Jean Pouilloux, pp. 303–319). Lyon, France: Maison de l'Orient Méditerranéen. (in French)

Hurst, D., & Freestone, I. (1996). Lead glazing technique from a medieval kiln site at Hanley Swan, Worcestershire. *Medieval Ceramics*, *20*, 13–18.

James, W. D., Dahlin, E. S., & Carlson, D. L. (2005). Chemical compositional studies of archaeological artifacts: Comparison of LA-ICP-MS to INAA measurements. *Journal of Radioanalytical and Nuclear Chemistry*, *263*, 697–702. DOI: 10.1007/s10967-005-0645-5.

Liu, Y. S., Hu, Z. C., Gao, S., Günther, D., Xu, J. A., Gao, C. G., & Chen, H. H. (2008). *In situ* analysis of major and trace elements of anhydrous minerals by LA-ICP-MS without applying an internal standard. *Chemical Geology*, *257*, 34–43. DOI: 10.1016/j.chemgeo.2008.08.004.

Maccabruni, C. (1987). Ceramica romana con invetriatura al piombo. In P. Lévęque, & J. P. Morel (Eds.), *Cèramiques hellenistique et romaines* (Annales scientifiques de l'Université de Besançon, pp. 167–182). Besancon, France: Université de Besançon. (in Italian)

Maccabruni, C. (1994). Ceramica invetriata con decorazione a rilievo. Nuovi ritrovamenti dal territorio pavese. *Rei Cretariae Romanae Fautores Acta*, *34*, 49–61. (in Italian)

Mangone, A., Giannossa, L. C., Laviano, R., Fioriello, C. S., & Traini, A. (2009). Investigations by various analytical techniques to the correct classification of archaeological finds and delineation of technological features: Late Roman lamps from *Egnatia*: From imports to local production. *Microchemical Journal*, *91*, 214–221. DOI:10.1016/j.microc.2008.11.006.

Mangone, A., De Benedetto, G. E., Fico, D., Giannossa, L. C., Laviano, R., Sabbatini, L., van der Werf, I. D., & Traini, A. (2011a). A multianalytical study of archaeological faience from Vesuvian area as a valid tool to investigate provenance and technological features. *New Journal of Chemistry*, *35*, 2860–2868. DOI: 10.1039/c1nj20626e.

Mangone, A., Giannossa, L. C., De Benedetto, G. E., Laviano, R., Traini, A., & Sabbatini, L. (2011b). Ceramica a pareti sottili da Ercolano: un'indagine archeometrica. In A. Coralini (Ed.), *Vesuviana.* Bologna, Italy: Antequem. (in Italian)

Martin, A. (1992). La ceramica invetriata romana: la testimonianza dell'Area NE delle Terme del Nuotatore ad Ostia. In L. Paroli (Ed.), *Proceedings of the Seminar at Certosa di Pontigliano*, February 23–24, 1990 (pp. 323–329). Firenze, Italy. (in Italian)

Molera, J., Pradell, T., Salvadó, N., & Vendrell-Saz, M. (2001). Interaction between clay bodies and lead glazes. *Journal of the American Ceramic Society*, *84*, 1120–1128. DOI: 10.1111/j.1151-2916.2001.tb00799.x.

Pérez-Arantegui, J., Uruñuela, M. I., & Castillo, J. R. (1996). Roman glazed ceramics in the Western Mediterranean: Chemical characterization by inductively coupled plasma atomic emission spectrometry of ceramic bodies. *Journal of Archaeological Science*, *23*, 903–914. DOI: 10.1006/jasc.1996.0085.

Picon, M., & Vichy, M. (1974). Recherches sur la composition des céramiques de Lyon. *Revue Archéologique de l'Est et du Centre-Est Consacrée aux Antiquités Nationales*, *25*(1), 37–59. (in French)

Picon, M., & Desbat, A. (1986). Note sur l'origine des céramiques à glaçure plombifère, généralement bicolore, des IIème et IIIème siècles, de Vienne et Saint-Romain-en-Gal, *Figlina*, *7*, 125–127. (in French)

Resano, M., Pérez-Arantegui, J., Garcia-Ruiz, E., & Vanhaecke, F. (2005). Laser ablation-inductively coupled plasma mass spectrometry for the fast and direct characterization of antique glazed ceramics. *Journal of Analytical Atomic Spectrometry*, *20*, 508–514. DOI: 10.1039/b500691k.

Šelih, V. S., & van Elteren, J. T. (2011). Quantitative multielement mapping of ancient glass using a simple and robust LA-ICP-MS rastering procedure in combination with image analysis. *Analytical & Bioanalytical Chemistry*, *401*, 745–755. DOI: 10.1007/s00216-011-5119-8.

Soricelli, G. (1988). Osservazioni intorno ad un cratere in ceramica invetriata da Pompei. *Rivista di Studi Pompeiani*, *1988*(II), 248–254. (in Italian)

Stoner, W. D., & Glascock, M. D. (2012). The forest or the trees? Behavioral and methodological considerations for geochemical characterization of heavily-tempered ceramic pastes using NAA and LA-ICP-MS. *Journal of Archaeological Science*, *39*, 2668–2683. DOI: 10.1016/j.jas.2012.04.011.

van Elteren, J. T., Tennent, N. H., & Šelih, V. S. (2009). Multielement quantification of ancient/historic glasses by laser ablation inductively coupled plasma mass spectrometry using sum normalization calibration. *Analytica Chimica Acta*, *644*, 1–9. DOI: 10.1016/j.aca.2009.04.025.

Walton, M. S., & Tite, M. S. (2010). Production technology of Roman lead-glazed pottery and its continuance into late antiquity. *Archaeometry*, *52*, 733–759. DOI: 10.1111/j.1475-4754.2009.00506.x.

Ziviello, V. (1989). Le terrecotte invetriate. In L. De Luca (Ed.), *Le collezioni del Museo Nazionale di Napoli* (pp. 204). Roma, Italy: Archivio fotografico Pedicini. (in Italian)